Optics Communications 465 (2020) 125647

Contents lists available at ScienceDirect

Optics Communications

journal homepage: www.elsevier.com/locate/optcom

High-quality factor, biological microsphere and microhemisphere lasers fabricated by a single solution process

Toan Van Nguyen [a,b], Van Duong Ta [c,*]

[a] Department of Physics, Le Quy Don Technical University, Hanoi 100000, Viet Nam
[b] Department of Quantum Optics, Faculty of Physics, VNU University of Science, Vietnam National University, Hanoi 100000, Viet Nam
[c] Department of Optical Devices, Le Quy Don Technical University, Hanoi 100000, Viet Nam

ARTICLE INFO

Keywords:
Biolasers
Spheres
Hemispheres
Whispering gallery mode
Dehydration

ABSTRACT

Whispering gallery mode (WGM) biological microlasers are attractive building blocks for developing biodegradable and implantable optical devices. To date, various biomaterials, laser configurations, and fabrication techniques have been investigated for WGM biolasers. However, the current technology is time-consuming and generally is not possible for fabricating various laser configurations in a single process. In this work, we demonstrate a unique technique that can produce micrometer-sized biolasers with two different geometries, microspheres and microhemispheres, in a short time of about 10 min. Using this technique, spheres and hemispheres with diameter from 20-100 μm can be fabricated easily from a dye-doped bovine serin albumin solution. The fabricated spheres and hemispheres can act as excellent lasers under optical pumping. The lasing threshold of the microsphere lasers is about 10 $\mu J/mm^2$ and their quality (Q) factor varies with size which can reach 3000 for a 90 μm-diameter sphere. The hemisphere lasers exhibit a slightly higher lasing threshold and lower Q factor.

1. Introduction

Biolasers are laser sources whose gain medium and/or cavity are made of biological materials. Biolasers have attracted extensive attention because of their wide-range applications in biosensing, tracking, labeling [1–3]. Current research on biolasers is exploring novel biomaterials, laser architectures, and fabrication techniques. To date, various biomaterials like proteins (fluorescent proteins, silk-based protein, bovine serin albumin), polysaccharides, DNA have been demonstrated as excellent candidates for biolasers [4]. Many laser architectures such as random cavities [5], Fabry–Perot [6], distributed feedback (DFB) [7] and whispering gallery mode (WGM) cavities [8–13] have also been explored for biolasers.

Generally, WGM cavities made of a circular or spherical transparent object such as sphere and disk [14]. WGM biolasers are particularly interesting due to their high quality (Q) factor, low lasing threshold, and simple fabrication. For example, a microsphere can be easily obtained by solution-based processes such as water-in-oil emulsion [11] or water-in-polydimethylsiloxane (PDMS) [12]. Microsphere lasers have been employed for intracellular biosensing and cell-tracking [15]. Another fascinating WGM laser is a hemisphere. Polymer-based hemisphere microlasers with various diameters can be fabricated on a planar substrate by using a top-down method [16,17]. The size and position of a hemisphere can be well controlled by an ink-jet system [18]. In addition, hemispheres are more stable than spheres when they are located on a substrate. The equator of a hemisphere-based cavity is located just above the topmost surface of the substrate. As a result, WGM of a hemisphere-based cavity can be coupled to a fiber taper which can be used for photonic integrated circuits (PICs) and optical sensors [19]. Despite these advantages, a hemisphere biolaser has not been investigated yet.

The fabrication techniques that have been developed for sphere and hemisphere lasers are generally different. For instance, the emulsion technique frequently used for making microspheres may not suitable for hemispheres [11,12]. To the best of our knowledge, a process for fabrication of both sphere and hemisphere microlasers has not been reported. In this work, we demonstrate a unique technique that allows obtaining biolasers with multiple laser architectures, in the form of sphere and hemisphere, in a single process. Lasing properties of these spheres and hemispheres are investigated and compared.

2. Experimental methods

2.1. Aqueous dye-doped bovine serin albumin solution

Bovine serin albumin (BSA, ≥ 98% purity), Rhodamine B (RhB, ≥ 95% dye) were purchased from Sigma-Aldrich. BSA solution was

* Corresponding author.
E-mail address: duong.ta@mta.edu.vn (V.D. Ta).

https://doi.org/10.1016/j.optcom.2020.125647
Received 3 February 2020; Received in revised form 26 February 2020; Accepted 27 February 2020
Available online 29 February 2020

prepared by dissolving 0.4 g of BSA in 0.5 mL deionized water. Subsequently, this BSA solution was mixed with 0.5 mL RhB solution 1 wt%. The BSA forms a cavity structure while RhB molecules provide emission.

2.2. Fabrication of microsphere and microhemisphere biolasers

We used water-in-decanol emulsion and dehydration to transfer aqueous microdroplets into solid spheres/hemispheres. Firstly, as shown in Fig. 1a, a micropipette is used to create a droplet (containing RhB, BSA, and water) in a glass beaker containing 5 mL 1-decanol (referred to decanol for convenience, ≥99% purity from Sigma-Aldrich). Subsequently, the droplet is gently stirred to form many microdroplets (Fig. 1b). Next, due to gravity, these droplets sink down to the bottom where two different substrates are located. The first substrate is a glass slide and the second substrate is also a glass slide but covered with a Teflon thread seal tape. Due to the difference in the surface wettability, droplets on the Teflon substrate (hydrophobicity) have spherical shapes (Fig. 1c) while droplets on the glass substrate (hydrophilicity) have hemispherical shapes (Fig. 1d). Then, as water is well dissolved in decanol, water molecules (inside the droplets) diffuse to the decanol (outer environment) until the dynamic equilibrium is established [20]. Finally, when this dehydration process is completed (all water molecules are removed from the droplets), solid-state microspheres on the Teflon substrate (Fig. 1e) [21] and hemispheres on the glass substrate (Fig. 1f) are obtained. In addition, for optical characterizations, the two substrates were taken out of the beaker and subsequently heated at 100 °C for 5 min. This process helps to remove completely the decanol from the hemispheres and spheres.

The transition (side view) from a typical protein droplet to a solid hemisphere/sphere can be seen in Fig. S1. It is noted that a large droplet size (around 1 mm in diameter) was chosen for the demonstration because it is easier (compared with a smaller droplet) to capture their images during the dehydration process.

2.3. Optical characterizations

Dynamic formation (top view) of a sphere/hemispheres from an aqueous droplet was studied by using an optical microscope (10× objective) combined with a camera. The camera captured the droplet (immersed in decanol) continuously after equal intervals of 6 s. By analyzing the obtained images, droplets' diameter can be determined. In this work, we used a MATLAB software for recognization of the droplets in the images and then calculates their diameter automatically.

A micro-photoluminescence (μ-PL) setup was used to study the obtained hemispheres and spheres. The pumping source was a Nd: YAG nanosecond pulse laser (Litron lasers) with a wavelength of 532 nm, a repetition rate of 10 Hz and a pulse duration of 4–7 ns. The spheres and hemispheres were excited by a focus laser beam with a spot size of ~350 μm in diameter. Emission from them was collected by a 10× objective and subsequently delivered to an AvaSpec-2048L (Avantes) for spectral recording. The spectral resolution of the spectrometer is 0.2 nm. All of the optical measurements were carried out in ambient conditions (in the air) and at room temperature.

3. Results and discussion

3.1. Dehydration process

Fig. 2a and b show the top-view optical microscope image of a typical droplet (~92 μm in diameter) on the glass and Teflon substrate during the dehydration process. Initially, they are in liquid form. However, due to the dehydration, the droplets' size decreases with time until they are solid.

The change in the droplets' size is shown in Fig. 2c. Starting with the same initial diameter of 92 μm, the two droplets decrease their size at a similar rate. However, the size of the droplet on the Teflon substrate decreases more than the droplet on the glass substrate. After 80 s, the diameter of the droplet on the Teflon substrate reduces to 67 μm, a 5 μm more, in comparison with 72 μm for the droplet on the glass substrate. The dehydration is completed after about 250 s. For a longer time, the equilibrium has already been established, their sizes are unchanged as they become solid. The final diameter of the hemisphere and sphere are 68 and 64 μm, respectively. Based on the final diameter of the sphere, the concentration of BSA in the solid hemisphere/sphere can be calculated, be around 1140 mg/mL. This value is consistent with previous works [20,22].

3.2. Dye-doped microsphere and microhemisphere biolasers

Obtained RhB-doped BSA spheres and hemispheres exhibit round shape with diameter from about 20 to 100 μm. The optical microscope image of the spheres shows uniform red color (Fig. 3a) which confirms the good incorporation of RhB molecules with the BSA cavity matrix. In addition, dark rings are visible are around the hemispheres due to the curvature of the spherical surface. Scanning electron microscope (SEM) image of the spheres on a Teflon substrate is presented in Fig. S2. For the convenience in optical characterizations, these spheres were transferred to a glass substrate and their SEM image is shown in Fig. 3b. It can be seen that the spheres show smooth surfaces which is necessary for good optical confinement and laser generation. The optical microscope and SEM image of the hemispheres are shown in Fig. 3c and Fig. 3d, respectively. The hemispheres also have round and smooth surfaces. It is noted that the dark rings do not observe around the hemispheres (in the optical image), which is probably due to their small curvature.

The advantages of our technique are simplicity, time-effectiveness, and flexibility. The fabrication process does not use any solvent and high-temperature annealing like the previous work [12]. The fabrication time is only around 10 min., at least one order of magnitude faster, compared with other methods such as evaporation or freeze-drying vacuum [13,23]. With regard to the flexibility, this method can produce not only microspheres but also different laser configuration such as hemispheres by just modifying the surface wettability. In addition, the output size of the hemispheres/spheres can be well controlled because the final diameter of the obtained hemispheres/spheres is directly related to the diameter of the initial droplets. If a microfluidic or ink-jet system can be used to create uniform initial droplets then mass production of monodisperse biolasers in the form of spheres and hemispheres can be achieved.

3.3. Lasing characteristics of a typical dye-doped BSA microsphere and microhemisphere biolasers

The RhB-doped spheres and hemispheres can work as excellent lasers under optical excitation. Fig. 4a and b show the photoluminescence (PL) emission spectra from a single sphere (~70 μm) and a single hemisphere (~74 μm) under different pump pulse energies (PPE). At low PPE (0. 32 μJ for the sphere and 0.46 μJ for the hemisphere), only spontaneous emission (low intensity and broad-spectrum) is obtained. At higher PPE (0.99 μJ) lasing peaks have appeared and are well recognized above the fluorescence background.

3.4. Comparison of optical properties between the sphere and hemisphere biolasers

Since this is the first-time microspheres/hemispheres-based lasers are made from the same material and conditions, it is interesting to compare their lasing properties. Fig. 5a and b show lasing emission spectra from a microsphere and a microhemisphere with a similar diameter of 43 μm. It can be seen that the two lasing spectra look almost the same with a free spectral range (FSR) of 2.0 nm. This observation

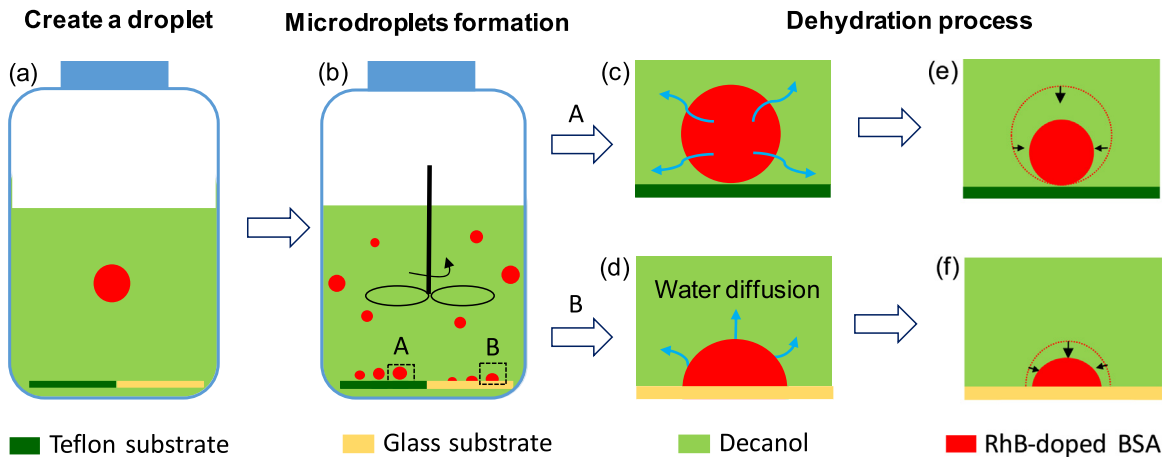

Fig. 1. Illustration of the fabrication process of hemisphere and sphere microlasers.

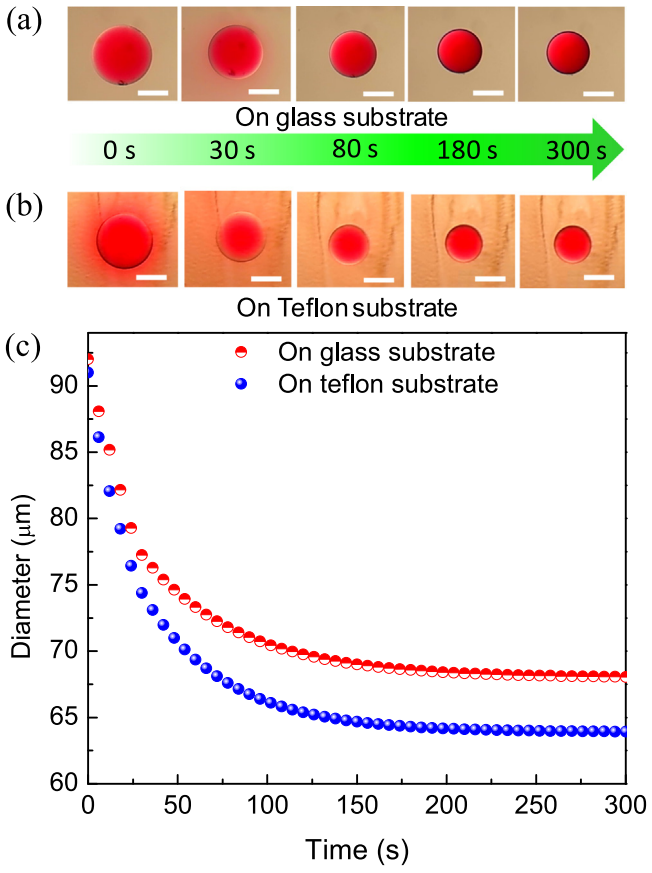

Fig. 2. Top-view optical image of a droplet on (a) a glass and (b) a Teflon substrate during the dehydration process in decanol. All scale bars are 50 μm. (c) The change in diameter of droplets on the glass and Teflon substrates as functions of time.

can be explained by the WGM mechanism. For a WGM laser, the FSR can be estimated as $\lambda^2/\pi nD$, where λ is the lasing wavelength, n and D is the refractive index and diameter of the sphere and hemisphere. In our case $n = 1.47$ [9], $D \approx 43$ μm, consider that $\lambda = 630$ nm then the calculated FSR is 1.95 nm, consistent with the experimental FSR of 2.0 nm. In addition, there is a slight difference in laser mode position between the two spectra, which can be clarified by the formula: $m\lambda = \pi Dn$, where m is the mode number and is determined to be 313 for the highest lasing mode of both sphere and hemisphere. As a result, the minor difference in the diameter explains the tiny variance in the position of the lasing modes of the sphere and hemisphere.

To provide a better view of the WGMs, we simulated the distribution of optical field intensity in the sphere/hemisphere by using the finite-element method (FEM) supported by COMSOL Multiphysics [24] and the result is shown in Fig. 5c and d. It can be seen that light is confined inside and near the equator of the sphere/hemisphere.

The integrated PL intensity of the sphere and hemisphere as a function of the pump pulse energy is shown in Fig. 5e. A distinct lasing threshold behavior is supported by the nonlinear increase in the emission intensity. The lasing threshold can be determined to be 0.90 μJ for the sphere and 1.10 μJ for the hemisphere. These values are equivalent to fluences of 9.4 μJ/mm^2 and 11.4 μJ/mm^2, respectively. The difference in the lasing threshold may be related to the optical

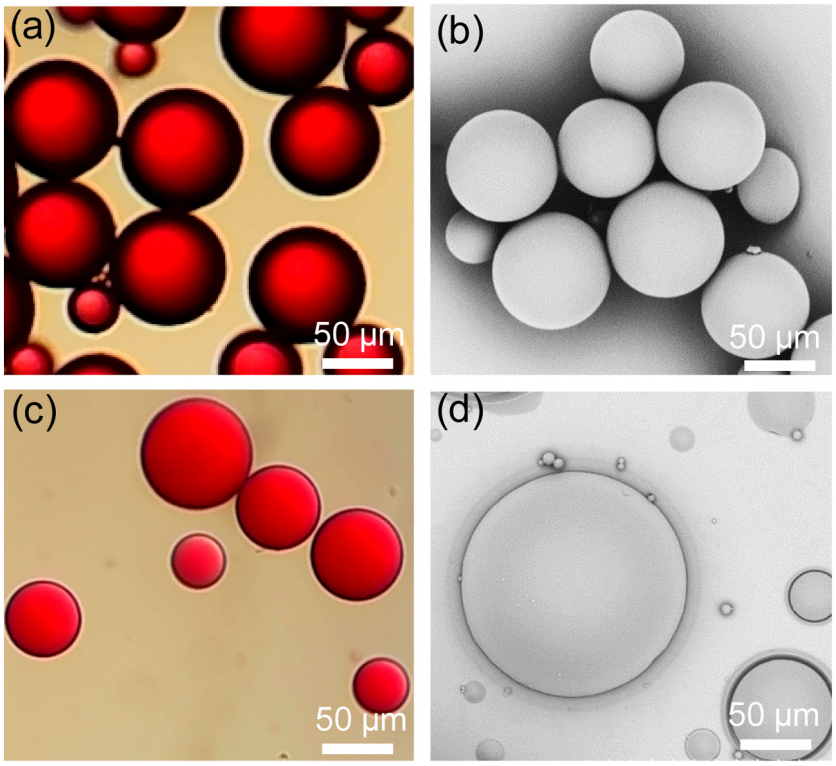

Fig. 3. Top-down optical and scanning electron microscope (SEM) image of RhB-doped BSA solid-state (a, b) spheres and (c, d) hemispheres on a glass substrate.. (For interpretation of the references to color in this figure legend, the reader is referred to the web version of this article.)

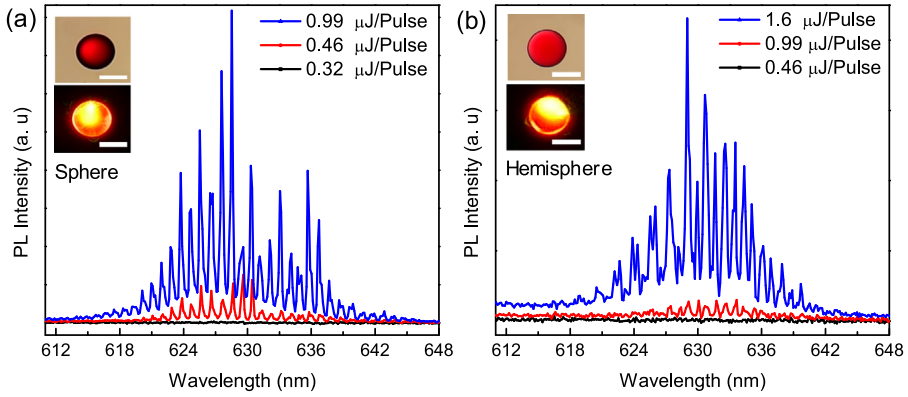

Fig. 4. PL spectrum of (a) a typical sphere and (b) a typical hemisphere under various pump pulse energies.

confinement or Q factor [25]. The Q factor of lasing modes is an important laser parameter and is defined as $Q = \lambda/\delta\lambda$, where $\delta\lambda$ is the full width at half maximum (FWHM) of the lasing mode. FWHM of the 43 μm-diameter sphere and hemisphere are 0.28 and 0.35 nm, respectively. Therefore, the Q factor is about 2230 for the sphere and 1790 for the hemisphere. The smaller Q factor of the hemisphere explains the higher lasing threshold in comparison with that of the sphere.

In order to get a statistic interpretation of the Q factor, 10 different spheres/hemispheres with various diameters were investigated and their Q factor is plotted in Fig. 6. It can be seen that the Q factor increases linearly with their diameters. For a similar size, the Q factor of a sphere is higher than that of a hemisphere. When the diameter increases from 28 to 91 μm, Q factors of the spheres rise from around 1800 to 3000 and 1500 to 2800 for the hemispheres. It is well-known that lower optical confinement or high optical loss leads to a lower Q factor. Herein, it is suggested that the optical leakage through a glass substrate is responsible for the smaller Q factor of the hemispheres [26]. However, the Q factor of hemispheres-based biolaser can be improved if replacing the glass substrate by a distributed Bragg reflector (DBR) that has a high reflection at emitted wavelength. In our previous work, the Q factor of hemispheres-based microlasers placed on a DBR can reach 6×10^3 [16].

The Q factor of the spheres/hemisphere is comparable to protein-based microdisk lasers [9], and nearly 3 times larger than starch-based ellipsoid lasers [13]. However, the microsphere biolasers in this work has a slightly lower Q factor compared to that in our previous study [12]. The reason may due to the difference in fabrication technique. In particular, a higher scattering loss (due to the surface inhomogeneity) may be responsible for the slight lower Q of the microspheres in this work.

4. Conclusion

In summary, we have demonstrated a simple but fast and effective technique for producing biolasers with multiple architectures. Two

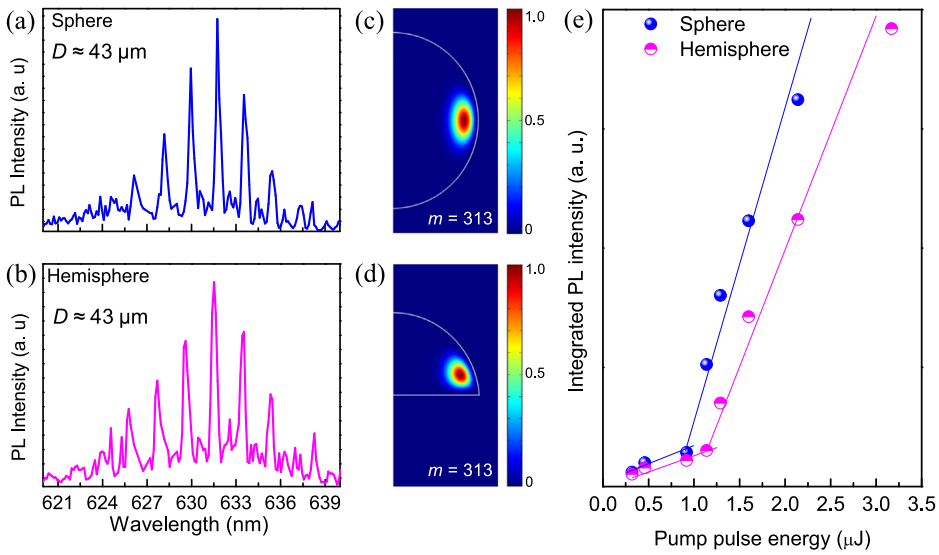

Fig. 5. PL spectrum of a sphere (a) and hemisphere (b) with nearly the same diameter of 43 μm. Distribution of electric field intensity inside a 43 μm-diameter sphere (c) and hemisphere (d). The integrated PL intensity of the sphere and hemisphere as a function of pump pulse energy.

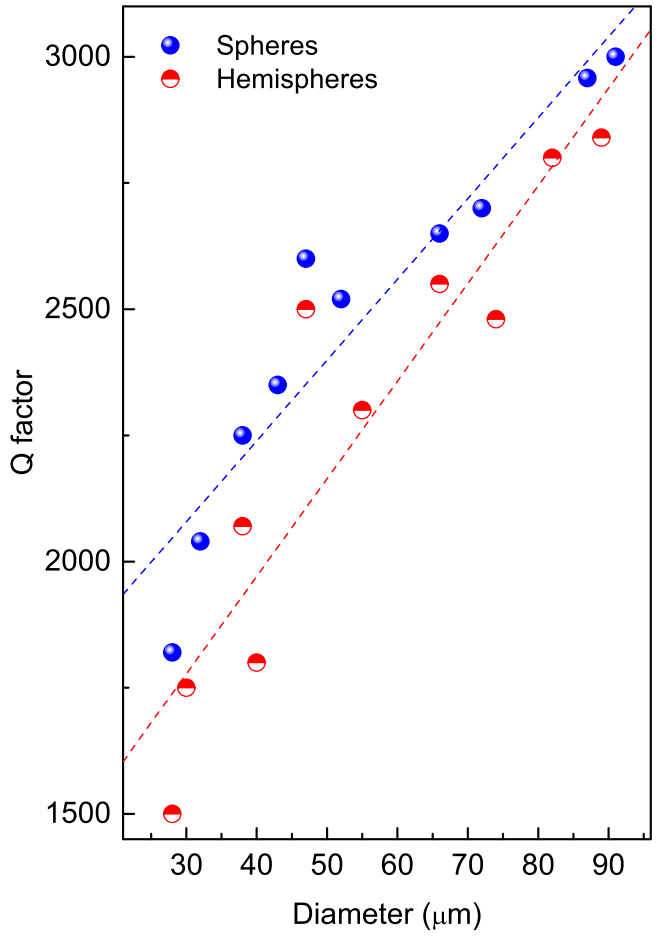

Fig. 6. Quality factor of spheres and hemispheres as functions of their diameter.

different laser configurations, microspheres and hemispheres, can be obtained in a single solution-based process and with a processing time of 10 min. By doping an organic dye into these structures, lasing emission was observed under optical pumping. Lasing properties of spheres and hemispheres have been investigated and compared. The lasing mechanism is ascribed to WGMs for both spheres and hemispheres. Generally, a sphere has a slightly lower lasing threshold and a higher Q factor compared with that of a hemisphere with a similar size. The lasing threshold of around 10 μJ/mm^2 and Q factor of lasing modes can be as high as 3×10^3 were obtained. This work presents an interesting and potentially useful method for the development of biological microlasers which is promising for biodegradable and implantable biosensors.

Declaration of competing interest

The authors declare that they have no known competing financial interests or personal relationships that could have appeared to influence the work reported in this paper.

Acknowledgment

This research is funded by Le Quy Don Technical University, Viet Nam under grant number 19.1.030.

References

[1] X. Fan, S.-H. Yun, The potential of optofluidic biolasers, Nature Methods 11 (2014) 141–147.
[2] V.D. Ta, Y. Wang, H. Sun, Microlasers enabled by soft-matter technology, Adv. Opt. Mater. 7 (2019) 1900057.
[3] Y.-C. Chen, X. Fan, Biological lasers for biomedical applications, Adv. Opt. Mater. 7 (2019) 1900377.
[4] J. Mysliwiec, K. Cyprych, L. Sznitko, A. Miniewicz, Biomaterials in light amplification, J. Opt. 19 (2017) 033003.
[5] S. Caixeiro, M. Gaio, B. Marelli, F.G. Omenetto, R. Sapienza, Silk-based biocompatible random lasing, Adv. Opt. Mater. 4 (2016) 998–1003.
[6] M.C. Gather, S.H. Yun, Single-cell biological lasers, Nature Photon. 5 (2011) 406–410.
[7] Y. Choi, H. Jeon, S. Kim, A fully biocompatible single-mode distributed feedback laser, Lab Chip 15 (2015) 642–645.
[8] S. Nizamoglu, M.C. Gather, S.H. Yun, All-biomaterial laser using vitamin and biopolymers, Adv. Mater. 25 (2013) 5943–5947.
[9] Y.-L. Sun, Z.-S. Hou, S.-M. Sun, B.-Y. Zheng, J.-F. Ku, W.-F. Dong, Q.-D. Chen, H.-B. Sun, Protein-based three-dimensional whispering-gallery-mode micro-lasers with stimulus-responsiveness, Sci. Rep. 5 (2015) 12852.
[10] Y.-C. Chen, Q. Chen, X. Fan, Lasing in blood, Optica 3 (2016) 809–815.
[11] M. Humar, A. Dobravec, X. Zhao, S.H. Yun, Biomaterial microlasers implantable in the cornea, skin, and blood, Optica 4 (2017) 1080–1085.
[12] V.D. Ta, S. Caixeiro, F.M. Fernandes, R. Sapienza, Microsphere solid-state biolasers, Adv. Opt. Mater. 5 (2017) 1601022.
[13] Y. Wei, X. Lin, C. Wei, W. Zhang, Y. Yan, Y.S. Zhao, Starch-based biological microlasers, ACS Nano 11 (2017) 597–602.

[14] M. Humar, Liquid-crystal-droplet optical microcavities, Liq. Cryst. 43 (2016) 1937–1950.
[15] M. Humar, S. Hyun Yun, Intracellular microlasers, Nature Photon. 9 (2015) 572–576.
[16] V.D. Ta, R. Chen, H.D. Sun, Self-assembled flexible microlasers, Adv. Mater. 24 (2012) OP60–OP64.
[17] V.D. Ta, R. Chen, D.M. Nguyen, H.D. Sun, Application of self-assembled hemispherical microlasers as gas sensors, Appl. Phys. Lett. 102 (2013) 031107.
[18] V.D. Ta, S. Yang, Y. Wang, Y. Gao, T. He, R. Chen, H.V. Demir, H. Sun, Multicolor lasing prints, Appl. Phys. Lett. 107 (2015) 221103.
[19] Z. Zhang, N. Yao, J. Pan, L. Zhang, W. Fang, L. Tong, A new route for fabricating polymer optical microcavities, Nanoscale 11 (2019) 5203–5208.
[20] Aniket D.A. Gaul, D.L. Rickard, D. Needham, MicroglassificationTM: A novel technique for protein dehydration, J. Pharm. Sci. 103 (2014) 810–820.
[21] T.V. Nguyen, N.V. Pham, H.H. Mai, D.C. Duong, H.H. Le, R. Sapienza, V.-D. Ta, Protein-based microsphere biolasers fabricated by dehydration, Soft Matter 15 (2019) 9721–9726.
[22] D.L. Rickard, P.B. Duncan, D. Needham, Hydration potential of lysozyme: protein dehydration using a single microparticle technique, Biophys. J. 98 (2010) 1075–1084.
[23] D. Venkatakrishnarao, M.A. Mohiddon, R. Chandrasekar, The photonic side of curcumin: Microsphere resonators self-assembled from curcumin derivatives emitting visible/near-infrared light, Adv. Opt. Mater. 5 (2017) 1600613.
[24] M. Oxborrow, Traceable 2-D finite-element simulation of the whispering-gallery modes of axisymmetric electromagnetic resonators, IEEE Trans. Microw. Theory Tech. 55 (2007) 1209–1218.
[25] L. He, Ş.K. Özdemir, L. Yang, Whispering gallery microcavity lasers, Laser Photonics Rev. 7 (2012) 1–23.
[26] R. Chen, V.D. Ta, H.D. Sun, Single mode lasing from hybrid hemispherical microresonators, Sci. Rep. 2 (2012) 244.